Evolution and global charge conservation for polarization singularities emerging from non-Hermitian degeneracies

Weijin Chen[a], Qingdong Yang[a], Yuntian Chen[a,b,1], and Wei Liu[c,1]

[a]School of Optical and Electronic Information, Huazhong University of Science and Technology, Hubei 430074, People's Republic of China; [b]Wuhan National Laboratory for Optoelectronics, Huazhong University of Science and Technology, Hubei 430074, People's Republic of China; and [c]College for Advanced Interdisciplinary Studies, National University of Defense Technology, Hunan 410073, People's Republic of China

Edited by Pablo G. Debenedetti, Princeton University, Princeton, NJ, and approved February 18, 2021 (received for review September 19, 2020)

Core concepts in singular optics, especially the polarization singularities, have rapidly penetrated the surging fields of topological and non-Hermitian photonics. For open photonic structures with non-Hermitian degeneracies in particular, polarization singularities would inevitably encounter another sweeping concept of Berry phase. Several investigations have discussed, in an inexplicit way, connections between both concepts, hinting at that nonzero topological charges for far-field polarizations on a loop are inextricably linked to its nontrivial Berry phase when degeneracies are enclosed. In this work, we reexamine the seminal photonic crystal slab that supports the fundamental two-level non-Hermitian degeneracies. Regardless of the invariance of nontrivial Berry phase (concerning near-field Bloch modes defined on the momentum torus) for different loops enclosing both degeneracies, we demonstrate that the associated far polarization fields (defined on the momentum sphere) exhibit topologically inequivalent patterns that are characterized by variant topological charges, including even the trivial scenario of zero charge. Moreover, the charge carried by the Fermi arc actually is not well defined, which could be different on opposite bands. It is further revealed that for both bands, the seemingly complex evolutions of polarizations are bounded by the global charge conservation, with extra points of circular polarizations playing indispensable roles. This indicates that although not directly associated with any local charges, the invariant Berry phase is directly linked to the globally conserved charge, physical principles underlying which have all been further clarified by a two-level Hamiltonian with an extra chirality term. Our work can potentially trigger extra explorations beyond photonics connecting Berry phase and singularities.

singular optics | Berry phase | polarization singularities | non-Hermiticity | photonic crystal slabs

Pioneered by Pancharatnam, Berry, Nye, and others (1–10), Berry phase and singularities have become embedded languages all across different branches of photonics. Optical Berry phase is largely manifested through either polarization evolving Pancharatnam–Berry phase or the spin-redirection Bortolotti–Rytov–Vladimirskii–Berry phase (2, 4, 5, 11–15); while optical singularities are widely observed as singularities of intensity (caustics) (6), phase (vortices) (7), or polarization (8–10). As singularities for complex vectorial waves, polarization singularities are skeletons of electromagnetic waves and are vitally important for understanding various interference effects underlying many applications (16–20).

There is a superficial similarity between the aforementioned two concepts: Both the topological charge of polarization field [Hopf index of line field (21, 22)] and Berry phase are defined on a closed circuit. Despite this, it is quite unfortunate that almost no definite connections have been established between them in optics. This is fully understandable: Berry phase is defined on the Pancharatnam connection (parallel transport) that decides the phase contrast between neighboring states on the loop (3, 4); while the polarization charge reflects accumulated orientation rotations of polarization ellipses, which has no direct relevance to the overall phase of each state. This explains why in pioneering works where both concepts were present (23–27), their interplay was rarely elaborated on.

Spurred by studies into bound states in the continuum, polarization singularities have gained enormous renewed interest in open periodic photonic structures, manifested in different morphologies with both fundamental and higher-order half-integer charges (28–50). Simultaneously, the significance of Berry phase has been further reinforced in surging fields of topological and non-Hermitian photonics (1, 23, 26, 51–56). In open periodic structures involving band degeneracies, Berry phase and polarization singularity would inevitably meet, which sparks the influential work on non-Hermitian degeneracy (36) and several other following studies (40, 43, 45) discussing both concepts simultaneously. Although not claimed explicitly, those works hint that nontrivial Berry phase produces nonzero polarization charges.

Aiming to bridge Berry phase and polarization singularity, we reexamine the seminal photonic crystal slab (PCS) that supports elementary two-level non-Hermitian degeneracies. It is revealed that with an invariant nontrivial π Berry phase, the

Significance

Relying on a two-level Hamiltonian with an extra chirality term, we establish subtle connections between Berry phase defined for near-field Bloch modes in open photonic crystal slabs and polarization singularities of their far-field radiations. With non-Hermitian degeneracies, it is revealed for different contours enclosing both degeneracies, despite a constant nontrivial π Berry phase, far-field polarization charges are variable in a discontinuous manner, which could even be the trivial zero. It is further revealed that the charge of the Fermi arc is actually not well defined, which could be different on opposite bands. Such seemingly complex evolutions of charge distributions are mediated by extra points of circular polarizations, which guarantee the global charge conservation that is consistent with Berry phase invariance.

Author contributions: Y.C. and W.L. designed research; W.C., Q.Y., and W.L. performed research; W.C., Y.C., and W.L. contributed new reagents/analytic tools; W.C., Q.Y., Y.C., and W.L. analyzed data; and W.L. wrote the paper.

The authors declare no competing interest.

This article is a PNAS Direct Submission.

[1]To whom correspondence may be addressed. Email: wei.liu.pku@gmail.com or yuntian@hust.edu.cn.

This article contains supporting information online at https://www.pnas.org/lookup/suppl/doi:10.1073/pnas.2019578118/-/DCSupplemental.

Published March 15, 2021.

corresponding polarization fields on different isofrequency contours enclosing both non-Hermitian degenerate points (or equivalently exceptional points [EPs]) (26) exhibit diverse patterns characterized by different polarization charges, even including the trivial zero charge. It is further revealed that the charge carried by the Fermi arc is actually not well defined, which could be different on opposite bands. We also discover that such complexity of field evolutions is constrained by global charge conservation for both bands, with extra points of circular polarizations (**C** points) playing pivotal roles. This reveals the explicit connection between globally conserved charge and the invariant Berry phase, underlying which the physical mechanisms have been further clarified by a two-level Hamiltonian with an extra chirality term (25). We show that such an unexpected connection is generically manifest in various structures, despite the fact that Berry phase and polarization charge actually characterize different entities of near-field Bloch modes and their projected far polarization fields, respectively: Bloch modes are defined on the momentum torus and can be folded into the irreducible Brillouin zone; while polarization fields are defined on the momentum sphere, due to the involvement of out-of-plane wave vectors along which there is no periodicity. Our study can spur further investigations in other subjects beyond photonics to explore conceptual interconnectedness, where both the concepts of Berry phase and singularities are present.

Results

For better comparisons, we revisit the rhombic-lattice PCS in ref. 36: refractive index n, side length p, height h, and tilting angle θ; semimajor (minor) diameters are l_1 (l_2); the whole structure is placed in an air background of $n=1$ (Fig. 1*A*; parameter values shown in the legend). We have further defined $\vartheta=\triangle l/l_2$ to characterize the mirror (k_x-k_z plane)-symmetry breaking when air holes are partially filled. When $\vartheta=0$, the dispersion surfaces (in terms of real parts of complex eigenfrequencies $\breve{\omega}=\breve{\omega}_1+i\breve{\omega}_2$ for the Bloch eigenmodes calculated with COMSOL Multiphysics) are presented in Fig. 1*B* (*SI Appendix*, section 1). Throughout this work, only transverse electric modes are studied and both frequency and wave vector are normalized: $\omega\rightarrow\omega p/2\pi c$ (c is light speed); $\mathbf{k}\rightarrow\mathbf{k}p/2\pi$. Both branch cut (Fermi arc) and branch points (EPs) on the isofrequency plane (position information shown in figure legends, as is the case throughout this work) are observed (marked also respectively in Fig. 1*C* by black curve and dots). If the two bands are characterized by $\breve{\omega}$ and $\breve{\omega}'$, at EPs $\breve{\omega}=\breve{\omega}'$ while at other positions on the Fermi arc $\breve{\omega}_1=\breve{\omega}_1'$ and $\breve{\omega}_2\neq\breve{\omega}_2'$. On the lower band, we have identified two **C** points (marked by stars; the corresponding eigenmodes are circularly polarized in the far field) on the isofrequency plane (position information shown in figure legends, as is the case throughout this work). Polarization fields (line fields in terms of the semimajor axis of the polarization ellipses) are projected on the Bloch vector k_x-k_y plane (Fig. 1*C*) (*SI Appendix*, section 1), with blue and red lines corresponding respectively to the eigenmodes on the lower and upper bands (fields exhibiting mirror symmetry as required by the structure symmetry). The characteristic non-Hermitian eigenvalue-swapping feature is further confirmed in Fig. 1*B*, where polarization fields are only continuous across the Fermi arc for opposite bands (25).

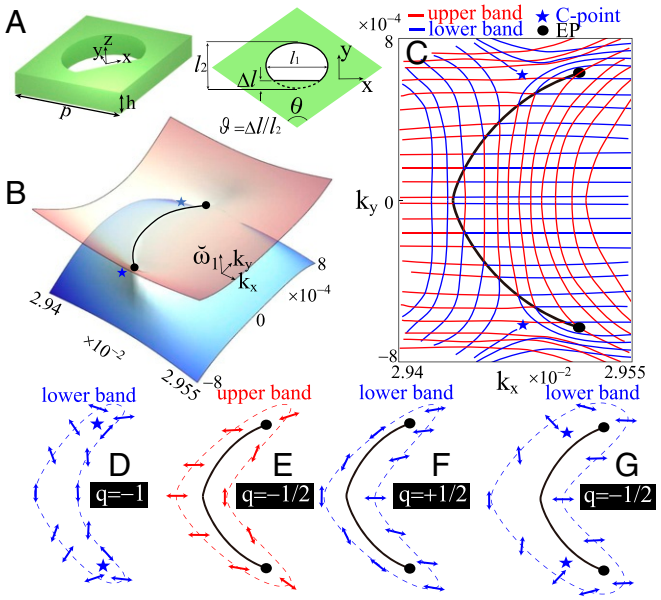

Fig. 1. (*A*) Unit cell of the rhombic-lattice PCS: index $n=1.384$, $p=525$ nm, $h=220$ nm, $l_1=348$ nm, $l_2=257$ nm, $\theta=114.5^\circ$, and $\vartheta=\triangle l/l_2$. (*B*) Dispersion surfaces ($\vartheta=0$) with two EPs $\breve{\omega}_1=0.961361$, $k_x=0.029525$, $k_y=\pm6.8\times10^{-4}$ and two **C** points on the lower band $\breve{\omega}_1=0.961347$, $k_x=0.029517$, $k_y=\pm6.8\times10^{-4}$. The polarization fields on a loop enclosing two **C** points are shown in *D* with $q=-1$. (*C*) Polarization fields for both lower (blue) and upper (red) bands. Three isofrequency contours are selected ($\breve{\omega}_1=0.961368, 0.961353, 0.96133$), on which the polarization fields are summarized in *E*–*G*, with $q=-1/2,\ +1/2,\ -1/2$, respectively.

The coexistence of two **C** points on the same band with equal charge $q=-1/2$ (generic polarization singularities) is protected by the mirror symmetry, decorated by typical star-like field patterns (57). On a contour that encloses two **C** points (without enclosing EPs), the polarization fields are shown in Fig. 1*D* with the expected charge $q=(-1/2)\times2=-1$. Such a contour is not on an isofrequency plane and thus not quite feasible for direct experimental verifications. We then proceed to isofrequency contours that are characterized by an invariant π Berry phase (58–62). Since both **C** points locate on the lower bands and on the isofrequency plane, for the upper band, there is no **C** point enclosed by the contour; for the lower band, the contour could enclose either zero or both **C** points simultaneously. Polarization fields on three such contours (one on the upper band [red dashed line] and two on the lower band [blue dashed lines]; double-headed arrows [equivalent to field lines] indicate the orientation of the semimajor axis of the polarization ellipses) are summarized in Fig. 1 *E*–*G*, with $q=-1/2,+1/2,-1/2$, respectively. The charge contrast of -1 between the two contours on the lower band is obviously induced by **C** points of total charge $q=-1$. It is clear from Fig. 1 *E* and *F* that the charge of the Fermi arc is not well defined, which is $q=\mp1/2$ on the upper and lower bands, respectively. The reason is that modes are only degenerate on EPs but not generally on the Fermi arc. In other words, the same Fermi arc actually corresponds to two sets of Bloch modes with polarization fields characterized by distinct charges.

Although we have studied the same structure ($\vartheta=0$) as that in ref. 36, our results presented in Fig. 1 are by no means mere reproductions, since the scenario of $q=+1/2$ we demonstrate is not covered in ref. 36, where the key roles of **C** points are also overlooked. We emphasize that although not explicitly demonstrated, the case of $q=+1/2$ was actually not forbidden by the arguments presented in ref. 36. Based on mode swapping and mirror symmetry properties, it was proved there that the charge associated with the isofrequency contour has to be a half-integer, accommodating both $q=\pm1/2$.

We then make a further step to investigate asymmetric structures ($\vartheta\neq0$). The polarization fields on the k_x-k_y plane for two scenarios ($\vartheta=0.01,\ 0.007$) are summarized in Fig. 2 *A* and *B*. With symmetry broken, although one **C** point on the lower band is relatively stable, the other can move to the Fermi arc (Fig. 2*B*) or across to the upper band (Fig. 2*A*), with invariant $q=-1/2$ (Table 1). When the two **C** points locate on opposite bands

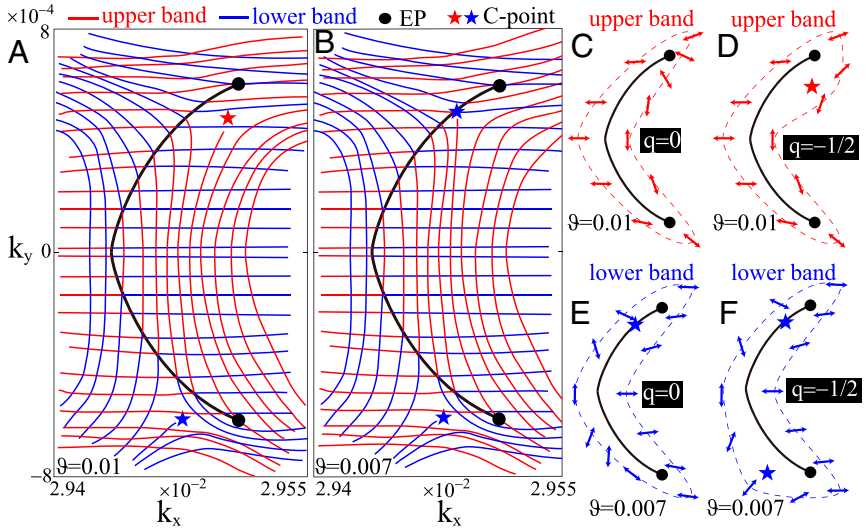

Fig. 2. (*A* and *B*) Polarization fields for two asymmetric PCSs with $\vartheta = 0.01$ and 0.007, respectively. The positions for the EPs are $\breve{\omega}_1 = 0.9612505$, $k_x = 0.029632$, $k_y = \pm 6.4 \times 10^{-4}$ in *A* and $\breve{\omega}_1 = 0.961297$, $k_x = 0.029592$, $k_y = \pm 6.6 \times 10^{-4}$ in *B*. The positions of the two **C** points are $\breve{\omega}_1 = (0.961261, 0.9612108)$, $k_x = (0.029638, 0.029623)$, $k_y = (6.3 \times 10^{-4}, -6.8 \times 10^{-4})$ in *A* and $\breve{\omega}_1 = (0.961297, 0.961270)$, $k_x = (0.029588, 0.02958)$, $k_y = (6.48 \times 10^{-4}, -6.8 \times 10^{-4})$ in *B*. In both *A* and *B*, two isofrequency contours are chosen, on which the polarizations fields are shown in *C*–*F*, with $q = 0, -1/2, 0, -1/2$ and $\breve{\omega}_1 = 0.9612 + (5.5, 8.3, 8.3, 5) \times 10^{-5}$, respectively.

(Fig. 2*A*), we choose two contours on the upper band (the charge distribution on the lower band is similar): One encloses two EPs only and the other encloses also the **C** point. The polarization fields on the contours are shown in Fig. 2 *C* and *D*, with $q = 0$ and $-1/2$, respectively. Despite this charge variance, we emphasize that for any isofrequency contour, the Berry phase is an invariant π, regardless of whether the symmetry is broken or not (58–62). Basically, Fig. 2*C* tells convincingly that a nontrivial Berry phase does not necessarily produce a nonzero polarization charge.

Except EPs, other points on the Fermi arc actually correspond to two sets of eigenmodes with equal $\breve{\omega}_1$ while different $\breve{\omega}_2$. As a result, the **C** point on the Fermi arc (Fig. 2*B*) is not really shared by both bands (only EPs are shared), but still locates on the lower band, which can be confirmed by inspecting $\breve{\omega}_2$. With the absence of **C** points, the charge distribution on the upper band would be identical to that in Fig. 1*B*: Any isofrequency contour encloses two EPs only with $q = -1/2$. On the lower band, in contrast, an isofrequency contour can enclose either two EPs and inevitably a **C** point on the Fermi arc or two EPs and two **C** points. Both scenarios are illustrated in Fig. 2 *E* and *F*, with $q = 0$ and $-1/2$, respectively. Fig. 2*E* reconfirms that Berry phase and partial polarization charge are not strictly interlocked.

Charge distributions for all three structures are summarized in Table 1, with blank spaces corresponding to scenarios not observed for structures studied in Fig. 1 or Fig. 2. Table 1 clearly indicates that for both the upper and lower bands, the global charge (when the contour is large enough to enclose not only EPs and but also all **C** points) is invariant ($q = -1/2$), irrespective of how the **C** points are distributed or whether the mirror symmetry is broken or not. In a word, there is a hidden order underlying the seemingly complex evolutions of polarization fields and their charges: The evolution is bounded by charge conservation. Considering the invariant π Berry phase for any isofrequency contours, it becomes clear that the global polarization charge (rather than partial ones when the contours cover part of the singularities of degeneracies or **C** points) is inextricably linked to this invariant Berry phase. Such a subtle connection is also subtly related to not only Hermitian degeneracies (25, 27, 45), but also scenarios with the degeneracies removed by further perturbations (25, 43).

As the final step, we employ the two-level Hamiltonian proposed in ref. 25 to clarify underlying physical mechanisms. The corresponding Hamiltonian of this model in the linear basis is

$$\mathcal{H}(k_x, k_y) = (k_x + i\gamma)\sigma_z + k_y\sigma_x + \kappa\sigma_y, \qquad [1]$$

where $k_{x,y}$ are real; $\sigma_{x,y,z}$ are Pauli matrices; and κ and γ are the planar chirality (*SI Appendix*, sections 2 and 3) and radiation loss terms, respectively. This Hamiltonian matrix is indeed a rather ordinary 2×2 non-Hermitian matrix, except that Berry and Dennis view its eigenvectors $\mathbf{x} = (x_1; x_2)$ as Jones vectors (63) to characterize polarized light (e.g., in linear basis $(1, \pm i)$ or equivalently $x_1 = \pm i x_2$ corresponds to circular polarizations). This establishes an effective connection between the Hamiltonian matrix and the electromagnetic polarization fields (*SI Appendix*, section 3). With this connection, when $\kappa = 0$, EPs correspond to degenerate eigenvectors satisfying $x_1^{\mathrm{EP}} = \pm i x_2^{\mathrm{EP}}$ and thus overlap with **C** points (chiral EPs); when $\kappa \neq 0$, EPs are nonchiral $x_1^{\mathrm{EP}} \neq \pm i x_2^{\mathrm{EP}}$ and thus separated from **C** points (25, 64–66). Since for realistic scenarios discussed in Figs. 1 and 2, all EPs are nonchiral, the introduction of chirality term κ is inevitable, which nevertheless is missing in ref. 36.

For convenience of analysis, to directly locate **C** points in particular, the Hamiltonian can be converted into a circular-basis form as (25)

Table 1. Charges for C points and different isofrequency contours (L and U, lower and upper bands, on which charge values are shown in blue and red colors, respectively)

	$\vartheta = 0$		$\vartheta = 0.01$		$\vartheta = 0.007$	
	L	U	L	U	L	U
1 C	−1/2		−1/2	−1/2	−1/2	
2 EPs	+1/2	−1/2	0	0		−1/2
2 EPs + 1 C			−1/2	−1/2	0	
2 EPs + 2 Cs	−1/2				−1/2	
Global	−1/2	−1/2	−1/2	−1/2	−1/2	−1/2

Entries underlined are scenarios covered in ref. 36.

$$\mathcal{H}_c(k_x,k_y)=(k_x+i\gamma)\sigma_x+k_y\sigma_y+\kappa\sigma_z$$
$$=\begin{pmatrix}\kappa & k_x-\mathrm{i}k_y+\mathrm{i}\gamma\\ k_x+\mathrm{i}k_y+\mathrm{i}\gamma & -\kappa\end{pmatrix}, \quad [2]$$

since such conversion would transform $\sigma_{x,y,z}$ in a linear basis to $\sigma_{y,z,x}$ in a circular basis (*SI Appendix*, section 2). After this conversion, circular-basis eigenvectors $x_1^c=\pm ix_2^c$ now correspond to linear polarizations, while those of $x_1^c x_2^c=0$ correspond to **C** points. Identical to the linear basis case, the EPs correspond to circular (noncircular) polarizations with the chirality term $\kappa=0$ ($\kappa\neq 0$). The superiority of this circular-basis Hamiltonian resides in that the positions of **C** points can then be directly identified by setting the off-diagonal terms of the matrix equal to zero: $k_x\pm\mathrm{i}k_y+\mathrm{i}\gamma=0$. Their roots $k_x=0,\ k_y=\mp\gamma$ are the positions of **C** points on the upper and lower bands, respectively (25). This model can explain the charge distributions shown in Fig. 2*A* (also summarized in Table 1 with $\vartheta=0.01$) with the two **C** points located on opposite bands, except that in this model the topological charge of the **C** point and the global charge for either band are $+1/2$ rather than $-1/2$ (*SI Appendix*, section 5). To account for these discrepancies, we modify the Hamiltonian as

$$\mathcal{H}_c(k_x,k_y)=(k_x+i\gamma)\sigma_x-k_y\sigma_y+\kappa\sigma_z, \quad [3]$$

the complex eigenvalues of which are $\breve{\eta}=\breve{\eta}_1+i\breve{\eta}_2=\pm\sqrt{k_x^2+k_y^2+\kappa^2-\gamma^2+2ik_x\gamma}$ ($\breve{\eta}$ is degenerate at EPs while only $\breve{\eta}_1$ is degenerate at other points on the Fermi arc). Eq. **3** is obtained by adding a minus sign before the σ_y term in Eq. **2**, which is similar to substituting the Hamiltonian of the K valley for that of the K′ valley in graphene, inducing a 2π jump of Berry phase from π to $-\pi$ (67, 68) (*SI Appendix*, sections 4 and 5). Although Berry phases of π and $-\pi$ are effectively the same (phase is only definable modulo 2π), the corresponding polarization fields and charge distributions are contrastingly different (*SI Appendix*, sections 4 and 5), with opposite signs for both the **C**-point charge and the global charge of both bands ($q=+1/2$ in Eq. **2** versus $q=-1/2$ in Eq. **3**). The polarization fields extracted from this modified model ($\gamma=1$ and $\kappa=0.8$) are shown in Fig. 3*A*, which are topologically equivalent to those in Fig. 2*A*: **C** points located on opposite bands with identical charge $q=-1/2$; for iso-eigenvalue ($\breve{\eta}_1$) contours that enclose both EPs, $q=-1/2$ and $q=0$ with and without the extra **C** point surrounded, respectively (Fig. 3 *C* and *D*); and the global charge is constant ($q=-1/2$) for both bands.

Since the model presented above is linear, there is only one solution when either off-diagonal term is setting to zero. This means that there is one and only one **C** point on each band. As a result, this linear model would fail to account for what is observed in Fig. 1*C*, where there are two **C** points on the same band. Actually, the linear model in Eq. **3** has broken the k_x-k_z mirror symmetry of the polarization fields on each band (represented by line fields of the same color), as confirmed by the field patterns in Fig. 3*A*. To reflect the mirror symmetry of the structure and thus also the polarization fields, the linear model can be further modified as

$$\mathcal{H}_c(k_x,k_y)=(k_x+i\gamma)\sigma_x-k_y\sigma_y-k_y\sigma_z, \quad [4]$$

where the constant chirality term κ in Eq. **3** is replaced by the variable $-k_y$, which guarantees that the constructed polarization fields are symmetric with respect to the k_x-k_z plane (see *SI Appendix*, section 6 for detailed arguments concerning field symmetry and this replacement). The symmetric fields on each band (in contrast to asymmetric ones in Fig. 3*A*) extracted from this model ($\gamma=1$ and $\kappa=0.8$) are shown in Fig. 3*B*, which is topologically equivalent to Fig. 1*C*: Two **C** points locate on the same band each with $q=-1/2$; for iso-eigenvalue contours on the upper band $q=-1/2$; iso-eigenvalue contours on the lower band that enclose both EPs have $q=+1/2$ and $q=-1/2$, without and with the two **C** points surrounded, respectively (Fig. 3 *E* and *F*); and the global charge is an invariant $q=-1/2$ for both bands. This reconfirms the claim in ref. 36: Combined mirror symmetry and mode swapping produce half-integer charges. Here for simplicity we have confined to linear models only, aiming to explain topologically what has been observed in Figs. 1 and 2. To obtain more than one **C** point on the same band, besides introducing the variable chirality term as shown in Eq. **4**, we can also incorporate nonlinear terms into the two-level Hamiltonian, which nevertheless would change the charge distribution both locally and globally (*SI Appendix*, section 7).

Conclusions

We revisit PCSs supporting EPs and establish a subtle connection between invariant Berry phase and the conserved global charge. It is revealed that for any isofrequency contour enclosing both EPs, despite the nontrivial π Berry phase invariance, the topological charge is contrastingly variable, which could even be the trivial zero charge. Such seemingly complex evolutions of charge

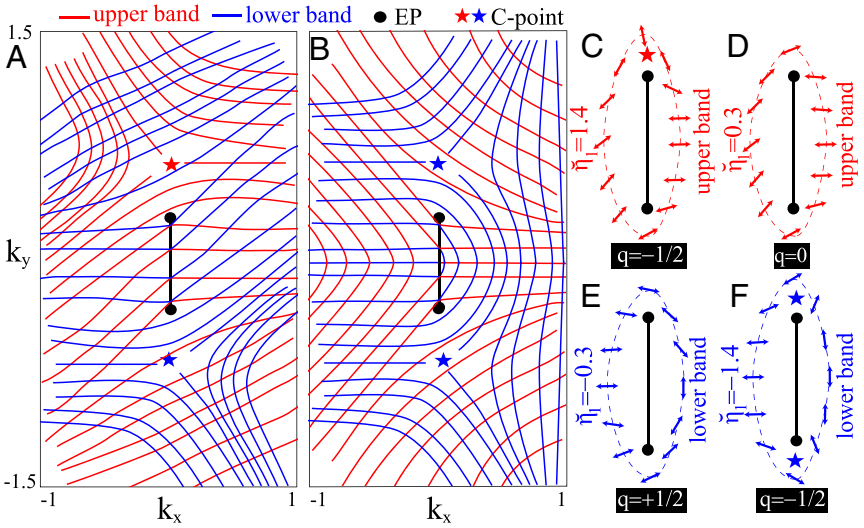

Fig. 3. (*A* and *B*) Polarization fields extracted from the model respectively in Eqs. **3** and **4**, with $\gamma=1$ and $\kappa=0.8$. Two iso-eigenvalue contours are selected in *A* and *B*, on which the polarizations fields are shown in *C*–*F*, with $q=-1/2, 0, +1/2, -1/2$, respectively.

distributions are mediated by extra **C** points, ensuring global charge conservation for both bands that is synonymous with the Berry phase invariance.

It is worth emphasizing that our Hamiltonians treat all modes as radiative (within the light cone), as indeed is the case throughout this work (*SI Appendix*, section 1). When the radiative term γ is sufficiently large, **C** points (located at $k_x = 0,\ k_y = \pm\gamma$) can move out of the light cone and thus become evanescent and not observable in the far field. Under this circumstance, those **C** points do not contribute to the global charge, which would then not be conserved anymore. Our discussions are confined to fundamental two-level systems, which can be extended to more sophisticated systems with more complex EP distributions (69–81). The Berry phase in this study is defined for near-field Bloch modes rather than their radiated electromagnetic fields, but it has recently been shown that the Berry phase for fields themselves on a contour can be also defined (14, 82). We expect that blending all those concepts (EPs, Berry phase of their matrix eigenvectors, Berry phase and polarization singularities of the corresponding electromagnetic waves) would render much more fertile platforms to incubate new fundamental investigations and practical applications, including the rare scenario of Berry phase (for electromagnetic fields) with slaving parameters (eigenvectors from which the electromagnetic fields are constructed) themselves also manifesting Berry phase.

Materials and Methods

For explicit descriptions of methods, refer to *SI Appendix*. Details concerning calculations of eigenmodes, their far polarization fields, and representations on the Bloch vector k_x-k_y plane are discussed in *SI Appendix*, section 1; transformations of Pauli matrices from the linear to the circular basis are presented in *SI Appendix*, section 2; the two-level Hamiltonian with an extra chirality term, its associated Berry phase, symmetry properties, and global topological charge of polarization fields are further elaborated on in *SI Appendix*, sections 3–6; a two-level Hamiltonian with nonlinear terms is discussed in *SI Appendix*, section 7; information concerning the handedness, charge, and line-field patterns of all **C** points discussed in our work is summarized in *SI Appendix*, section 8 (*SI Appendix*, Fig. S4).

Data Availability. All study data are included in this article and/or *SI Appendix*.

ACKNOWLEDGMENTS. We acknowledge the financial support from the National Natural Science Foundation of China (Grants 11874026 and 11874426), and the Outstanding Young Researcher Scheme of the National University of Defense Technology. W.L. is grateful to M. V. Berry for invaluable correspondences.

1. S. Pancharatnam, The propagation of light in absorbing biaxial crystals. *Proc. Indian Acad. Sci. U.S.A.* **42**, 86–109 (1955).
2. S. Pancharatnam, Generalized theory of interference, and its applications. *Proc. Indian Acad. Sci. U.S.A.* **44**, 247–262 (1956).
3. M. V. Berry, Quantal phase factors accompanying adiabatic changes. *Proc. R. Soc. A* **392**, 45–57 (1984).
4. M. V. Berry, The adiabatic phase and Pancharatnam phase for polarized-light. *J. Mod. Opt.* **34**, 1401–1407 (1987).
5. M. Berry, Geometric phase memories. *Nat. Phys.* **6**, 148–150 (2010).
6. M. V. Berry, Waves and Thom's theorem. *Adv. Phys.* **25**, 1–26 (1976).
7. J. F. Nye, M. V. Berry, Dislocations in wave trains. *Proc. R. Soc. Lond. A* **336**, 165–190 (1974).
8. J. F. Nye, Polarization effects in the diffraction of electromagnetic waves: The role of disclinations. *Proc. R. Soc. A* **387**, 105–132 (1983).
9. J. F. Nye, Lines of circular polarization in electromagnetic wave fields. *Proc. R. Soc. A* **389**, 279–290 (1983).
10. M. V. Berry, "Geometry of phase and polarization singularities illustrated by edge diffraction and the tides" in *Second International Conference on Singular Optics (Optical Vortices): Fundamentals and Applications*, M. S. Soskin, M. V. Vasnetsov, Eds. (SPIE Europe, Cardiff, United Kingdom, 2001), vol. 4403, pp. 1–12.
11. E. Bortolotti, Memories and notes presented by fellows. *Rend. R. Acc. Naz. Linc.* **4**, 552 (1926).
12. S. M. Rytov, Transition from wave to geometrical optics. *Dokl. Akad. Nauk. SSSR* **18**, 263 (1938).
13. V. V. Vladimirskii, The rotation of polarization plane for curved light ray. *Dokl. Akad. Nauk. SSSR* **21**, 222 (1941).
14. K. Y. Bliokh, M. A. Alonso, M. R. Dennis, Geometric phases in 2D and 3D polarized fields: Geometrical, dynamical, and topological aspects. *Rep. Prog. Phys.* **82**, 122401 (2019).
15. E. Cohen *et al.*, Geometric phase from Aharonov–Bohm to Pancharatnam–Berry and beyond. *Nat. Rev. Phys.* **1**, 437–449 (2019).
16. M. R. Dennis, K. O'Holleran, M. J. Padgett, "Chapter 5 singular optics: Optical vortices and polarization singularities" in *Progress in Optics*, E. Wolf, Ed. (Elsevier, 2009), Vol. 53, pp. 293–363.
17. G. J. Gbur, *Singular Optics* (CRC Press, Boca Raton, FL, 2016).
18. M. Burresi *et al.*, Observation of polarization singularities at the nanoscale. *Phys. Rev. Lett.* **102**, 033902 (2009).
19. A. B. Young *et al.*, Polarization engineering in photonic crystal waveguides for spin-photon entanglers. *Phys. Rev. Lett.* **115**, 153901 (2015).
20. F. Cardano, E. Karimi, L. Marrucci, C. de Lisio, E. Santamato, Generation and dynamics of optical beams with polarization singularities. *Opt. Express* **21**, 8815–8820 (2013).
21. H. Hopf, *Differential Geometry in the Large: Seminar Lectures New York University 1946 and Stanford University 1956* (Springer, 2003).
22. T. Needham, *Visual Differential Geometry and Forms: A Mathematical Drama in Five Acts* (Princeton University Press, 2021).
23. M. Berry, Pancharatnam, virtuoso of the Poincaré sphere: An appreciation. *Curr. Sci.* **67**, 220 (1994).
24. M. Berry, Making waves in physics. *Nature* **403**, 21 (2000).
25. M. V. Berry, M. R. Dennis, The optical singularities of birefringent dichroic chiral crystals. *Proc. R. Soc. Lond. A* **459**, 1261–1292 (2003).
26. M. Berry, Physics of nonhermitian degeneracies. *Czech. J. Phys.* **54**, 1039–1047 (2004).
27. M. V. Berry, M. R. Jeffrey, "Chapter 2 conical diffraction: Hamilton's diabolical point at the heart of crystal optics" in *Progress in Optics*, E. Wolf, Ed. (Elsevier, 2007), vol. 50, pp. 13–50.
28. C. W. Hsu, B. Zhen, A. D. Stone, J. D. Joannopoulos, M. Soljačić, Bound states in the continuum. *Nat. Rev. Mater.* **1**, 16048 (2016).
29. C. W. Hsu *et al.*, Observation of trapped light within the radiation continuum. *Nature* **499**, 188–191 (2013).
30. B. Zhen, C. W. Hsu, L. Lu, A. D. Stone, M. Soljačić, Topological nature of optical bound states in the continuum. *Phys. Rev. Lett.* **113**, 257401 (2014).
31. Y. Yang, C. Peng, Y. Liang, Z. Li, S. Noda, Analytical perspective for bound states in the continuum in photonic crystal slabs. *Phys. Rev. Lett.* **113**, 037401 (2014).
32. Y. Guo, M. Xiao, S. Fan, Topologically protected complete polarization conversion. *Phys. Rev. Lett.* **119**, 167401 (2017).
33. A. Kodigala *et al.*, Lasing action from photonic bound states in continuum. *Nature* **541**, 196–199 (2017).
34. E. N. Bulgakov, D. N. Maksimov, Topological bound states in the continuum in arrays of dielectric spheres. *Phys. Rev. Lett.* **118**, 267401 (2017).
35. H. M. Doeleman, F. Monticone, W. den Hollander, A. Alù, A. F. Koenderink, Experimental observation of a polarization vortex at an optical bound state in the continuum. *Nat. Photon.* **12**, 397 (2018).
36. H. Zhou *et al.*, Observation of bulk Fermi arc and polarization half charge from paired exceptional points. *Science* **359**, 1009–1012 (2018).
37. Y. Zhang *et al.*, Observation of polarization vortices in momentum space. *Phys. Rev. Lett.* **120**, 186103 (2018).
38. K. Koshelev, S. Lepeshov, M. Liu, A. Bogdanov, Y. Kivshar, Asymmetric metasurfaces with high-Q resonances governed by bound states in the continuum. *Phys. Rev. Lett.* **121**, 193903 (2018).
39. W. Chen, Y. Chen, W. Liu, Singularities and Poincaré indices of electromagnetic multipoles. *Phys. Rev. Lett.* **122**, 153907 (2019).
40. A. Chen *et al.*, Observing vortex polarization singularities at optical band degeneracies. *Phys. Rev. B* **99**, 180101 (2019).
41. W. Liu *et al.*, Circularly polarized states spawning from bound states in the continuum. *Phys. Rev. Lett.* **123**, 116104 (2019).
42. J. Jin *et al.*, Topologically enabled ultrahigh-Q guided resonances robust to out-of-plane scattering. *Nature* **574**, 501–504 (2019).
43. C. Guo, M. Xiao, Y. Guo, L. Yuan, S. Fan, Meron spin textures in momentum space. *Phys. Rev. Lett.* **124**, 106103 (2020).
44. X. Yin, J. Jin, M. Soljačić, C. Peng, B. Zhen, Observation of topologically enabled unidirectional guided resonances. *Nature* **580**, 467–471 (2020).
45. W. Ye, Y. Gao, J. Liu, Singular points of polarizations in the momentum space of photonic crystal slabs. *Phys. Rev. Lett.* **124**, 153904 (2020).
46. W. Chen, Y. Chen, W. Liu, Line singularities and Hopf indices of electromagnetic multipoles. *Laser Photon. Rev.* **14**, 2000049 (2020).
47. Z. Liu *et al.*, High-Q quasibound states in the continuum for nonlinear metasurfaces. *Phys. Rev. Lett.* **123**, 253901 (2019).
48. C. Huang *et al.*, Ultrafast control of vortex microlasers. *Science* **367**, 1018–1021 (2020).
49. B. Wang *et al.*, Generating optical vortex beams by momentum-space polarization vortices centered at bound states in the continuum. *Nat. Photon.* **14**, 623–628 (2020).
50. T. Yoda, M. Notomi, Generation and annihilation of topologically protected bound states in the continuum and circularly polarized states by symmetry breaking. *Phys. Rev. Lett.* **125**, 053902 (2020).
51. L. Lu, J. D. Joannopoulos, M. Soljacic, Topological photonics. *Nat. Photon.* **8**, 821 (2014).
52. T. Ozawa *et al.*, Topological photonics. *Rev. Mod. Phys.* **91**, 015006 (2019).
53. L. Feng, R. El-Ganainy, L. Ge, Non-Hermitian photonics based on parity–time symmetry. *Nat. Photon.* **11**, 752–762 (2017).
54. R. El-Ganainy *et al.*, Non-Hermitian physics and PT symmetry. *Nat. Phys.* **14**, 11–19 (2018).

55. M. A. Miri, A. Alù, Exceptional points in optics and photonics. *Science* **363**, eaar7709 (2019).
56. T. Wu *et al.*, Vector exceptional points with strong superchiral fields. *Phys. Rev. Lett.* **124**, 083901 (2020).
57. M. V. Berry, J. H. Hannay, Umbilic points on Gaussian random surfaces. *J. Phys. Math. Gen.* **10**, 1809–1821 (1977).
58. M. Berry, Two-state quantum asymptotics. *Ann. N. Y. Acad. Sci.* **755**, 303–317 (1995).
59. A. A. Mailybaev, O. N. Kirillov, A. P. Seyranian, Geometric phase around exceptional points. *Phys. Rev. A* **72**, 014104 (2005).
60. O. N. Kirillov, "Non-Hermitian perturbation of Hermitian matrices" in *Nonconservative Stability Problems of Modern Physics* (De Gruyter, ed. 1, 2013), chap. 11.5.
61. D. Leykam, K. Y. Bliokh, C. Huang, Y. D. Chong, F. Nori, Edge modes, degeneracies, and topological numbers in non-hermitian systems. *Phys. Rev. Lett.* **118**, 040401 (2017).
62. H. Shen, B. Zhen, L. Fu, Topological band theory for non-hermitian Hamiltonians. *Phys. Rev. Lett.* **120**, 146402 (2018).
63. A. Yariv, P. Yeh, *Photonics: Optical Electronics in Modern Communications* (Oxford University Press, ed. 6, New York, NY, 2006).
64. W. Heiss, H. Harney, The chirality of exceptional points. *Eur. Phys. J. D* **17**, 149–151 (2001).
65. H. L. Harney, W. D. Heiss, Time reversal and exceptional points. *Eur. Phys. J. D* **29**, 429–432 (2004).
66. M. V. Berry, Proximity of degeneracies and chiral points. *J. Phys. Math. Gen.* **39**, 10013–10018 (2006).
67. C. L. Kane, E. J. Mele, Quantum spin Hall effect in graphene. *Phys. Rev. Lett.* **95**, 226801 (2005).
68. D. Xiao, W. Yao, Q. Niu, Valley-contrasting physics in graphene: Magnetic moment and topological transport. *Phys. Rev. Lett.* **99**, 236809 (2007).
69. W. D. Heiss, Chirality of wavefunctions for three coalescing levels. *J. Phys. Math. Theor.* **41**, 244010 (2008).
70. J. W. Ryu, S. Y. Lee, S. W. Kim, Analysis of multiple exceptional points related to three interacting eigenmodes in a non-Hermitian Hamiltonian. *Phys. Rev. A* **85**, 042101 (2012).
71. S. Y. Lee, J. W. Ryu, S. W. Kim, Y. Chung, Geometric phase around multiple exceptional points. *Phys. Rev. A* **85**, 064103 (2012).
72. W. D. Heiss, G. Wunner, Resonance scattering at third-order exceptional points. *J. Phys. Math. Theor.* **48**, 345203 (2015).
73. Z. Lin, A. Pick, M. Lončar, A. W. Rodriguez, Enhanced spontaneous emission at third-order Dirac exceptional points in inverse-designed photonic crystals. *Phys. Rev. Lett.* **117**, 107402 (2016).
74. W. D. Heiss, G. Wunner, A model of three coupled wave guides and third order exceptional points. *J. Phys. Math. Theor.* **49**, 495303 (2016).
75. W. Chen, Ş. Kaya Özdemir, G. Zhao, J. Wiersig, L. Yang, Exceptional points enhance sensing in an optical microcavity. *Nature* **548**, 192–196 (2017).
76. H. Hodaei *et al.*, Enhanced sensitivity at higher-order exceptional points. *Nature* **548**, 187–191 (2017).
77. X. L. Zhang, S. Wang, B. Hou, C. T. Chan, Dynamically encircling exceptional points: In situ control of encircling loops and the role of the starting point. *Phys. Rev. X* **8**, 021066 (2018).
78. E. J. Pap, D. Boer, H. Waalkens, Non-Abelian nature of systems with multiple exceptional points. *Phys. Rev. A* **98**, 023818 (2018).
79. K. Ding, G. Ma, Z. Q. Zhang, C. T. Chan, Experimental demonstration of an anisotropic exceptional point. *Phys. Rev. Lett.* **121**, 085702 (2018).
80. X. L. Zhang, C. T. Chan, Hybrid exceptional point and its dynamical encircling in a two-state system. *Phys. Rev. A* **98**, 033810 (2018).
81. Q. Zhong, M. Khajavikhan, D. N. Christodoulides, R. El-Ganainy, Winding around non-Hermitian singularities. *Nat. Commun.* **9**, 4808 (2018).
82. M. V. Berry, P. Shukla, Geometry of 3D monochromatic light: Local wavevectors, phases, curl forces, and superoscillations. *J. Optic.* **21**, 064002 (2019).